Advances in Analytic Science 2025, 6(1), 3670.
https://doi.org/10.54517/aas3670

Article

Geochemistry and source area weathering of soils around Mount Bamboutos (Cameroon Volcanic Line)

Lemnyuy Prosper Yiika[1,*], Adze Rene Meniemoh[2], Emmanuel Eseya Mengu[3], Chin Thierry Berinyuy[3], Kouankap Nono Gus Djibril[2]

[1] Department of Geology, Mining and Environmental Science, The University of Bamenda, P.O. Box 39, Bamenda, North West Region, Cameroon
[2] Department of Geology, Higher Teachers Training College Bambili, The University of Bamenda, P.O. Box 039, Bamenda, North West Region, Cameroon
[3] Department of Geology, Faculty of Science, University of Buea, P.O. Box 63, Buea, South West Region, Cameroon
*** Corresponding author:** Lemnyuy Prosper Yiika, lemnyuyprosper@gmail.com

CITATION

Yiika LP, Meniemoh AR, Mengu EE, et al. Geochemistry and source area weathering of soils around Mount Bamboutos (Cameroon Volcanic Line). Advances in Analytic Science. 2025; 6(1): 3670. https://doi.org/10.54517/aas3670

ARTICLE INFO

Received: 29 April 2025
Accepted: 4 June 2025
Available online: 17 June 2025

Abstract: This study aimed at investigating the weathering of the source area and the geochemistry of the soils around Mount Bamboutos, West Region, Cameroon. In this study, soil samples were collected from a depth of 0–40 cm. The soil samples were analyzed using inductively coupled plasma mass spectrometry (ICP-MS). Significant SiO_2 (63.37–73.05 wt.%) content recalculated to an anhydrous basis and adjusted to 100% (SiO_2 (adj)) indicates the abundance of quartz and kaolinite in soil samples. The enrichment of Al_2O_3 (9.98–15.12 wt.%) suggests the presence of aluminosilicate minerals such as clay minerals, muscovite, and feldspars. The considerable Fe_2O_3 (0.01–11.04 wt.%) content relates to the mechanical erosion of ferrallitic soil or to Fe-source rock weathering. The elevated LaN/YbN levels indicate that the soils were derived from heterogeneous source rocks during weathering. The inverse correlation between SiO_2 and Fe_2O_3, MgO, TiO_2, and P_2O_5 indicates the prevalence of heavy minerals, which are likewise influenced by the relative amount of quartz. The positive Ce anomalies may result from the redox conditions. Weathering indices such as the plagioclase index of alteration (PIA: 77.03%–97.75%), Chemical Index of Weathering (CIX: 58.25%–66.83%), chemical weathering index (CIW: 91.31%–99.13%), and chemical index of alternation (CIA: 50%–70%) all signify moderate to intense weathering in the source area, which occurred in hot, humid climatic conditions. This is evidenced by the removal of labile cations (Ca, Na, and K) in relation to stable residual components (Al and Ti). The relatively high Ce anomalies in the soil samples (Ce/Ce* = 0.01 to 7.44; average 2.39) suggest intense chemical weathering.

Keywords: soils; weathering indices; redox conditions; pedogenesis; Mount Bamboutos; Cameroon

1. Introduction

Soil is a non-renewable weathering product that is formed by the lengthy pedogenesis process that rocks go through. Cameroon is known for its wide variety of soil types, which are the result of the parent materials' long-term interactions with the climate, organisms, and terrain [1,2]. The survival of humans and the integrity of ecosystems depend heavily on soils [3]. Characteristics such as parent material, topographical position, slope steepness, moisture distribution, flora, and the age of the surrounding landscape contribute to the variations in soils found in different geologic formations [4]. The soil will alter wherever one or more of these crucial components change [5]. Several studies have been conducted to ascertain the

contents of trace metals in soils, water, and sediments, which have been identified as sinks for these environmental media [6–16]. Assessing weathering indices is crucial for determining soil fertility, soil erosion, rock weathering, and the availability of vital nutrients that are derived from rock weathering. These factors have an impact on agriculture and may have environmental repercussions [17]. Plagioclase Index of Alteration (PIA), Ruxton index, Chemical Index of Alteration (CIA vs. CIX), Chemical Index of Weathering (CIW), and Index of Compositional Variability (ICV) are some of the parameters used to evaluate weathering intensity of soils. These indices are helpful in assessing the extent of weathering that has taken place throughout the soil formation process [18]. Several researchers have documented the formation, nature, chemistry, and mineralogy of the soils around Mount Bamboutos, Cameroon [19–26]. Nevertheless, little is known about the geochemistry and source area weathering of soils around Mount Bamboutos in Cameroon. The current study focuses on geochemistry and source area weathering, which are both fundamental to research, and also aims to advance knowledge of source area weathering of soils in Cameroon.

2. Geologic setting

Mount Bamboutos, which ranges in elevation from 200 m to 2700 m above sea level, is located between latitudes 5°44′ and 5°36′ N and longitudes 9°55′ and 10°07′ E in the Cameroon Volcanic Line. The Cameroon Volcanic Line (CVL; **Figure 1**) contains Mount Bamboutos. Oceanic and continental volcanic massif alignments and orogenic plutonic complexes comprise the CVL [21]. Among the massifs that comprise the continental portion of the CVL is Mount Bamboutos. Rocks including basalts, hawaiites, mugearites, phonolites, trachytes, and ignimbrites are found in Mount Bamboutos, a notable polygenetic volcano along the CVL [22,23]. Mount Mélétan (2740 m) is the summit of the undulating chain of volcanoes that makes up the Bambouto volcano. Between 1.8 and 4.5 million years ago, volcanic activity produced basic lava flows and highly differentiated lavas in Mount Bamboutos [24]. Along the CVL, ignimbritic deposits are identified only in its continental portion, primarily within Mount Bamboutos [25]. Lava from Mount Bamboutos has K-Ar and Ar-Ar dates ranging from 21.12 to 0.5 Ma [25,26].

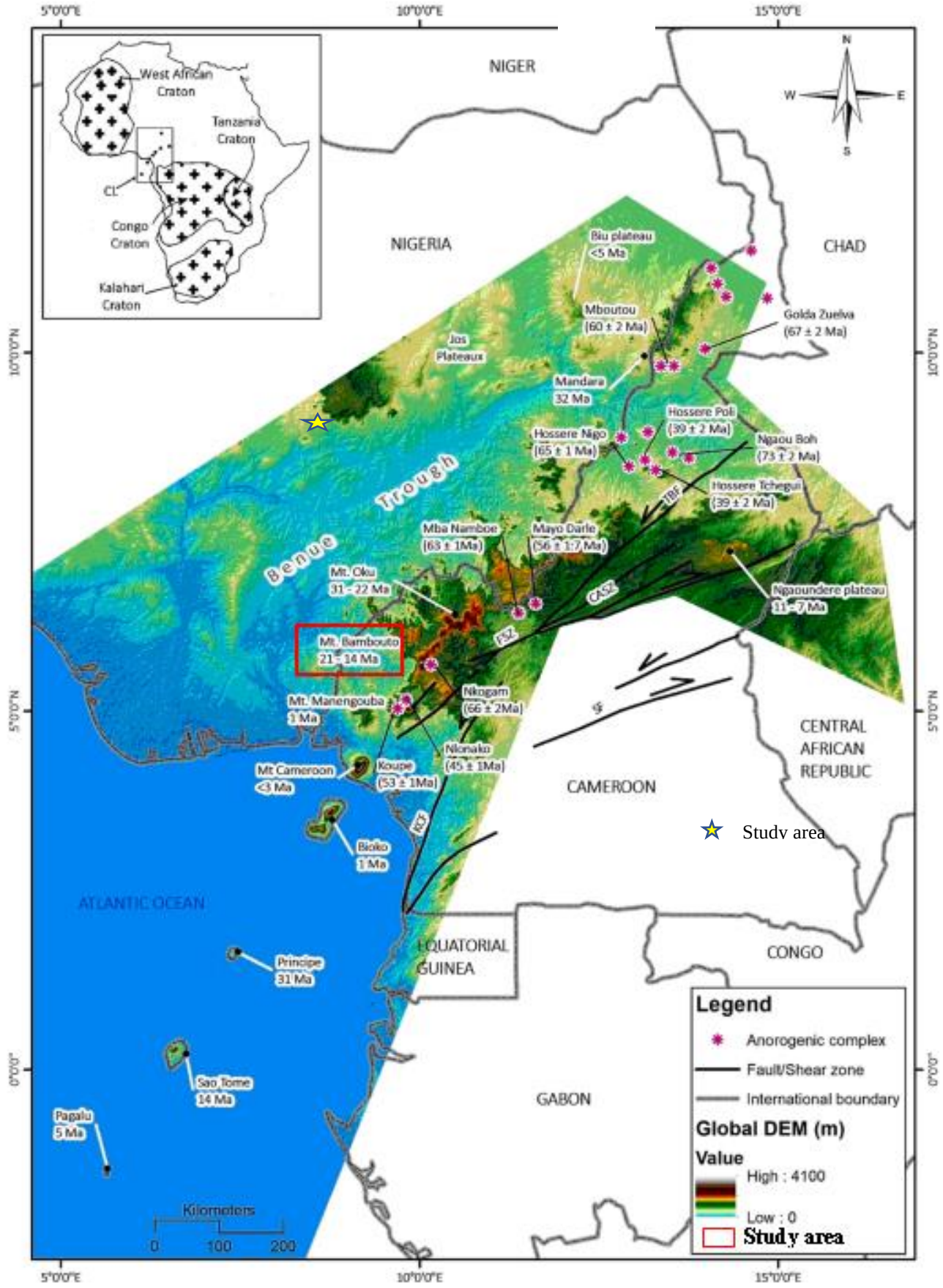

Figure 1. Morphotectonic map of the Cenozoic Cameroon Volcanic Line and age data of some volcanoplutonic complexes.

.

3. Materials and method

Using a stainless-steel shovel, soil samples weighing 1 kg each were methodically collected at a depth of 0–40 cm. After being carefully marked, the soil samples were put in polythene bags. The soil samples were air-dried, then mixed, crushed using a pestle in a porcelain mortar, sieved through a 2 mm sieve, and kept in polythene bags for chemical analysis. Aqua regia (9 mL HNO_3, 3 mL HCl) was used to digest 0.5 g of soil sample in a Perkin Elmer Multivalve 3000 Microwave. The microwave was set to 160 ℃ for 10 min and kept there for 15 min using 800 W of power and 30 bar of pressure. A Perkin Elmer Nexion 300Q ICP-MS was used for ICP-MS analysis and digestion of various soil samples at Activation Laboratories (ACTLABS) Ltd., Ontario, Canada. Using analytical-grade chemicals and reagents, glassware and vessels were rinsed with 20% HNO_3 and allowed to air-dry after rinsing with deionized water. The microwave-assisted digestion was carried out for 35 min at a rate of 0.5 bar s^{-1}. Following the microwave-assisted digestion, the samples were filtered and transferred into distilled water. Replicate method blanks and standard reference material (UME EnvCRM 03) were used to accomplish quality control and assurance. Microsoft Excel and the statistical package for social science (SPSS 16.0) were used for statistical analysis. The relative standard deviations for the triplicate samples were within ±10% of the mean, while the recoveries for major, trace, and rare earth elements (REE) ranged from 95% to 105%. The chemical data for major, trace, and rare earth elements in this study were normalized using upper continental crust (UCC) [27], Post-Archean Australian shales [27], and chondrite-normalized [28]. Adjusted to 100%, the (SiO_2) adj. denotes SiO_2 contents that have been recalculated to an anhydrous base. This study used the following weathering index methods: plagioclase alteration index (PIA), chemical alteration index (CIA), modified chemical alteration index (CIX), and chemical weathering index (CIW).

$$CIA = 100 \times [Al_2O_3/(Al_2O_3 + CaO^* + Na_2O + K_2O)] \text{ [29]} \quad (1)$$

$$ICV = (Fe_2O_3 + K_2O + Na_2O + CaO + MgO + MnO)/Al_2O_3) \text{ [30]} \quad (2)$$

$$CIW\ (\%) = [Al_2O_3/(Al_2O_3) + CaO^* + Na_2O] \text{ X } 100 \text{ [31]} \quad (3)$$

$$PIA\ (\%) = [(Al_2O_3 - K_2O)\ /(Al_2O_3 + CaO^* + Na_2O - K_2O)] \times 100 \quad (4)$$

$$CIX = (A1_2O_3/(A1_2O_3 + Na_2O + K_2O)] \times 100 \quad (5)$$

$$\text{Ruxton index} = SiO_2\ (adj)/Al_2O_3 \text{ ratio [32]} \quad (6)$$

4. Results and discussion

4.1. Major element geochemistry

Table 1 summarizes the major oxide concentrations in soil samples. The soil samples show high concentrations of Fe_2O_3 (0.01 to 11.04 wt.%), Al_2O_3 (9.98 to 15.12 wt.%), and SiO_2 (adj) (63.37 to 73.05 wt.%). The concentration of K_2O was slightly enriched in all the soil samples (0.01 to 9.93 wt%). TiO_2, MgO, MnO, P_2O_5, CaO, and Na_2O are present at low concentrations in all the soil samples. The concentrations of SiO_2 (adj), Al_2O_3 and Fe_2O_3 were above the Upper Continental Crust (UCC) and Post-Archean Australian Shale (PAAS) values [27]. The abundant SiO_2 contents suggest the presence of a high proportion of quartz and kaolinite. They may also have been linked to the clay mineral structure in accord with the weathering of source rocks. The significant enrichment of Fe_2O_3 implies that the soil is derived from Fe-rich source rocks [33]. Considerable content of Al_2O_3 indicates the presence of clay minerals, feldspars, and muscovite in soil samples [16,34]. The high SiO_2 and significant Al_2O_3 contents indicate a higher compositional maturity. Due to clay mineral alteration and neoformation, the low plagioclase feldspar content and other minerals are likely associated with the low contents of CaO, MgO, MnO, K_2O and Na_2O in comparison to UCC and PAAS threshold values [33,34]. The depletion in alkali and alkaline earth oxide contents may be linked to the low feldspar contents, high mobility during weathering, or during the sorting. The inverse relationships between SiO_2 (adj) and Al_2O_3 suggest that the proportion of quartz in the soils mostly determines its principal element composition (**Table 2**) [35]. The moderate correlation between Fe_2O_3/CaO (r = 0.68) and Fe_2O_3/MnO (r = 0.53) indicates that soils contain mafic minerals. According to the correlation of major oxides, soil samples around Mount Bamboutos may contain phyllosilicates, clay minerals, minerals containing iron, and apatite (**Table 2**) [34]. SiO_2 has a statistically insignificant correlation with Na_2O and K_2O (r = −0.16 and −0.99, respectively) (**Table 2**), indicating the high mobility of Na and K during clay material weathering and neoformation [36]. There is a notable association between Zr and Hf (r = 0.99; **Table 2**). This association suggests that zircon controls Hf in the soils. The Al_2O_3 and Th association is statistically significant (r = 0.69), indicating that the distribution of phyllosilicates is controlled by Th [37]. The inverse correlation between SiO_2 and Fe_2O_3, MgO, TiO_2, and P_2O_5 indicates the prevalence of heavy minerals such as garnet, amphibole, and apatite, which are likewise influenced by the relative amount of quartz. The strong relationships between Al_2O_3, Fe_2O_3, and K_2O indicate that the majority of Al_2O_3 was linked to heavy minerals such as garnets and amphiboles as well as clay minerals, K-rich feldspar, and mica [38].

Table 1. Concentrations of major oxides (wt. %) and major oxide ratios in soil samples.

	H1	**H2**	**H3**	**H4**	**H5**	**H6**	**H7**	**H8**	**H9**	**H10**	**H11**	**H12**
SiO_2 (adj)	73.05	68.42	66.16	74.90	66.85	99.92	63.37	63.90	64.60	69.24	64.27	68.27
Al_2O_3	10.64	13.51	14.66	9.98	15.12	0.02	14.57	15.1	15.12	12.47	15.12	15.12
Fe_2O_3	7.92	9.05	9.69	7.12	9.01	0.01	11.04	10.4	10.12	8.95	10.38	8.26
MgO	0.21	0.18	0.03	0.07	0.06	0.01	0.08	0.06	0.10	0.14	0.08	0.13
CaO	0.05	0.08	0.18	0.06	0.37	0.00	0.35	0.27	0.26	0.29	0.31	0.11
Na_2O	0.50	0.04	0.07	0.14	0.07	0.01	0.08	0.33	0.14	0.15	0.04	0.07
K_2O	**7.12**	8.14	8.72	6.41	8.10	0.01	9.93	9.42	9.11	8.05	9.34	7.44

TiO_2	0.01	0.01	0.01	0.01	0.01	0.00	0.02	0.01	0.02	0.03	0.01	0.01
MnO	0.23	0.38	0.30	0.45	0.28	0.02	0.28	0.25	0.25	0.40	0.18	0.28
P_2O_5	0.26	0.18	0.18	0.82	0.13	0.00	0.28	0.19	0.29	0.28	0.26	0.32
SiO_2 (adj)/Al_2O_3	6.87	5.06	4.51	7.51	4.42	5288.07	4.35	4.23	4.27	5.55	4.25	4.52
K_2O/Na_2O	14.37	204.77	128.43	44.70	118.66	99.63	124.26	28.94	62.98	53.77	215.92	111.82
CIA %	58.09	62.05	62.06	60.15	63.88	56.31	58.43	60.16	61.38	59.49	60.92	66.51
PIA%	86.51	97.85	96.07	94.65	94.07	77.03	91.45	90.58	93.73	90.94	94.18	97.75
CIW	95.10	99.13	98.37	98.02	97.16	91.31	97.11	96.23	97.41	96.59	97.69	98.85
CIX	58.25	62.28	62.52	60.37	64.91	59.25	59.27	60.81	62.03	60.32	61.70	66.83

Table 2. Pearson's correlation coefficient of major (%. wt) and trace elements (ppm).

	SiO_2 (adj)	**Al_2O_3**	**Fe_2O_3**	**MgO**	**CaO**	**Na_2O**	**K_2O**	**TiO_2**	**MnO**	**P_2O_5**	**Rb**	**Ba**	**Sr**	**Th**	**U**	**Zr**	**Hf**	**Y**	**Nb**	**Sc**
SiO_2 (adj)	1																			
Al_2O_3	−0.99	1																		
Fe_2O_3	−0.99	**0.96**	1																	
MgO	−0.26	0.22	0.26	1																
CaO	−0.67	**0.65**	**0.68**	−0.20	1															
Na_2O	−0.16	**0.08**	0.19	0.48	−0.12	1														
K_2O	−0.99	**0.96**	1.00	0.26	**0.68**	0.19	1													
TiO_2	−0.62	**0.55**	**0.63**	0.45	0.44	0.23	0.63	1												
MnO	−0.54	**0.51**	**0.53**	0.37	0.12	0.08	**0.53**	**0.74**	1											
P_2O_5	−0.19	0.13	0.18	0.12	−0.15	0.14	0.18	0.33	**0.66**	1										
Rb	−0.35	0.34	0.32	0.13	−0.19	0.26	0.32	0.41	**0.70**	0.82	1									
Ba	−0.49	0.46	0.48	**0.52**	−0.09	0.19	0.48	0.36	**0.62**	0.46	0.45	1								
Sr	−0.15	0.18	0.12	**0.55**	−0.48	0.16	0.12	0.05	0.40	0.38	0.42	**0.86**	1							
Th	−0.65	**0.69**	**0.63**	0.17	0.24	0.12	**0.63**	0.16	0.27	−0.29	0.12	0.30	0.17	1						
U	−0.85	**0.85**	**0.82**	0.25	0.39	0.43	**0.82**	**0.53**	0.45	0.21	**0.57**	0.31	0.15	**0.67**	1					
Zr	−0.52	**0.62**	0.46	−0.28	**0.60**	−0.19	0.46	0.03	0.08	−0.27	−0.02	−0.05	−0.14	**0.60**	0.47	1				
Hf	−0.50	**0.60**	0.44	−0.31	**0.57**	−0.24	0.44	0.00	0.11	−0.27	−0.03	0.03	−0.07	**0.61**	0.41	**0.99**	1			
Y	−0.46	0.41	0.48	**0.76**	−0.15	**0.73**	0.48	0.28	0.34	0.19	0.33	**0.65**	**0.63**	0.47	**0.55**	−0.03	−0.06	1		
Nb	−0.48	0.49	0.47	−0.14	**0.70**	−0.15	0.47	0.23	−0.07	−0.03	−0.07	−0.41	−0.53	0.07	0.42	0.41	0.30	−0.22	1	
Sc	−0.83	**0.78**	**0.86**	0.11	**0.73**	−0.02	**0.86**	**0.56**	0.28	−0.12	−0.04	0.35	−0.07	**0.52**	**0.54**	0.30	0.31	0.21	0.40	1

4.2. Trace element geochemistry

The concentrations of trace elements in the soil samples are listed in **Table 3**. The trace element data was compared with PAAS and UCC values. Hf, Sc, Y, Zr, V, Cu, Rb, U, and Th generally showed depletion when compared with UCC and PAAS threshold values. Ni (0.10–72.10 ppm) and Co (0.10–28.90 ppm) transition element

concentrations were enriched in comparison to UCC and PAAS values, indicating a felsic source. High field strength elements (HFSE) range from 0.3 to 130.40, and large ion lithophile elements (LILE) range from 1.37 to 284.30, indicating a low-moderate level of LILE enrichment in soil samples. The low to moderate levels of LILE suggest their incorporation in sheet silicates, such as illite and illite-smectite, and sorption onto clay mineral surfaces. The low LILE contents might also relate to the basaltic nature of source rocks. HFSE and LILE, such as Zr, Th, U, Hf, Y, and Rb, have concentrations below the UCC and PAAS standards. In the study area, transition elements Co, Cr, V, and Ni were more abundant than UCC and PAAS values. The soil samples contain readily leachable plagioclase feldspar; hence, the depletion of Sr in the soil samples was likely attributable to weathering.

Table 3. Concentration of trace elements (ppm) and selected elemental ratios in soil samples.

	H1	**H2**	**H3**	**H4**	**H5**	**H6**	**H7**	**H8**	**H9**	**H10**	**H11**	**H12**
Rb	12.5	9.6	17.1	26.8	7.4	0.1	5.9	13.4	15.5	13.2	8.7	17.2
Ba	120	131	97.5	120	57.5	0.5	155	68.9	73.5	66.9	43.2	141
Sr	88.9	80.1	54	70.7	10.7	0.5	59.8	6.7	14.5	10.7	13.1	116
Th	7.2	12.7	12.8	2.3	9.7	0.1	5.6	11.2	8.2	4	6.1	7.3
U	2.7	2.2	3.1	2.2	2.4	0.1	1.8	3.5	2.9	2.5	2.8	2.8
Zr	16.1	23.4	68.7	9.2	105	0.1	29	43.4	33	22.5	45.7	48.8
Hf	0.2	0.4	0.9	0.2	1.3	0.1	0.5	0.6	0.4	0.3	0.5	0.7
Y	31.4	19.2	15.1	13	10.1	0.01	14.6	14.8	13.8	10.2	11.8	14.8
Nb	0.5	2	3.7	3.6	14	0.1	4.9	12.2	13.4	12.7	28.8	6.3
Sc	4.8	9.4	9.9	2.7	6.6	0.1	14.9	11.2	10.9	10	10.2	7.1
V	52	66	72	51	58	2	126	88	97	108	95	60
Cr	21	55	50	28	33	1	119	64	67	79	70	41
Co	15.3	11.8	9.6	8.1	9	0.1	16.7	28.9	16.7	15.8	10.3	8.5
Cu	8.9	16	14.1	13.3	12.2	0.2	29.6	31.9	30.4	33.9	31.2	15.2
Ni	15.8	36	34.6	17.9	28.7	0.1	72.1	57.2	45.7	40.6	33.9	29.1
Zn	92.3	78.4	68.2	99.3	129	0.1	74.7	82.2	112	104	87.7	90.4
∑LILE	231.3	235.6	184.5	222	87.7	1.3	228.1	103.7	114.6	97.3	73.9	284.3
∑HSE	48.2	45	88.4	26	130.4	0.31	49	71	60.6	45.7	86.8	70.6
∑TTE	210.1	272.6	258.4	220.3	276.5	3.6	453	363.4	379.7	391.3	338.3	251.3
Th/U	2.67	5.77	4.13	1.05	4.04	1.00	3.11	3.20	2.83	1.60	2.18	2.61

4.3. Rare earth element geochemistry

Table 4 presents the rare earth elements found in the soil samples. The soil total REE concentrations range from 1.63 to 423.70 parts per million, consistent with lithological characteristics. The abundances of heavy and light REE (LaN/YbN =

0.32 to 45.73) in soil samples show varying fractionation. In comparison to heavy rare earth elements (HREE; GdN/YbN = 0.50 to 4.33), light rare earth elements (LREE: La, Ce, Pr, Nd, and Sm) are enriched $(La/Sm)_N$ = 0.76 to 9.94). The origin of soils from diverse parent rocks during weathering (basaltic and felsic rocks) is responsible for the marginally significant LaN/YbN levels. The significant (La/Yb)N values might be relative to the high fractionation of REE during weathering and erosion [29]. The majority of soil samples displayed a positive cerium anomaly (Ce/Ce* ≈ 0.83 to 7.44) and a consistently positive europium anomaly (Eu/Eu* = 0.25 to 4.34). The positive Ce anomalies may result from the redox conditions.

Table 4. Concentrations of rare earth elements (ppm) and elemental ratios.

	H1	**H2**	**H3**	**H4**	**H5**	**H6**	**H7**	**H8**	**H9**	**H10**	**H11**	**H12**
La	105	85.7	53.3	56.7	39	0.5	66.9	34.3	39.3	23.5	30.4	68.6
Ce	172	220	210	116	106	0.01	133	169	130	72.1	116	170
Pr	22.6	18.2	12.7	10.1	7.7	0.1	14.7	9	9.4	6.3	8	13.1
Nd	83.3	61	45.6	36.1	28.9	0.02	58.4	38.2	38.1	26.8	33	47.8
Sm	11.5	9.5	6.7	5.4	4.2	0.1	10.4	6.5	7.2	4.7	5.9	6.9
Eu	2.5	1.9	1.6	1.3	1.1	0.1	2.5	1.5	1.6	1.1	1.4	1.5
Gd	10.2	8.2	6.6	4.9	4	0.1	8	6.2	6	4.2	5.2	6.2
Tb	1.4	1	0.8	0.7	0.5	0.1	1	0.8	0.8	0.6	0.7	0.8
Dy	7	4.9	4.3	3.4	2.5	0.1	5	4.1	4	3	3.5	4.1
Ho	1.2	0.8	0.7	0.6	0.4	0.1	0.8	0.7	0.7	0.5	0.6	0.7
Er	3.4	2.5	2.1	1.6	1.3	0.1	1.9	2.1	1.9	1.4	1.6	2
Tm	0.4	0.3	0.3	0.2	0.2	0.1	0.2	0.3	0.2	0.2	0.2	0.2
Yb	2.8	2.1	1.6	1.1	1	0.1	1.2	1.9	1.6	1.2	1.2	1.5
Lu	0.4	0.3	0.2	0.2	0.2	0.1	0.2	0.3	0.2	0.2	0.2	0.2
ΣREE	423.7	416.4	346.5	238.3	197	1.63	304.2	274.9	241	145.8	207.9	323.6
ΣLREE	291.9	310.6	276.6	168.9	147.9	0.33	219	224.2	186.3	111	164.3	239.3
ΣHREE	26.8	20.1	16.6	12.7	10.1	0.8	18.3	16.4	15.4	11.3	13.2	15.7
LREE/HREE	10.89	15.45	16.66	13.3	14.64	0.41	11.97	13.67	12.1	9.82	12.45	15.24
(La/Yb)N	2.42	2.63	2.15	3.33	2.52	0.32	3.6	1.16	1.58	1.26	25.33	45.73
(Gd/Yb)N	1.82	1.95	2.06	2.23	2	0.5	3.33	1.63	1.88	1.75	4.33	4.13
(Ce/Sm)N	1.12	1.73	2.34	1.6	1.88	0.01	0.95	1.94	1.35	1.14	19.66	24.64
(La/Sm)N	1.38	1.37	1.21	1.59	1.41	0.76	0.98	0.8	0.83	0.76	5.15	9.94
Eu/Eu*	1	0.93	1.04	1.1	1.16	4.34	1.19	1.02	1.06	1.07	0.25	0.23
Ce/Ce*	0.83	1.31	1.9	1.14	1.44	0.01	1	2.27	1.59	1.4	7.44	5.67
La/La*	1	0.87	0.86	1.15	1.13	0.4	1.14	1.14	1.1	1.12	−0.72	−1.22

LREE = La, Ce, Pr, Nd, Sm, and Eu; HREE = Gd, Tb, Dy, Ho, Er, Tm, Yb, and Lu.

$$Ce/Ce^{*}cn = (Cesample/Cechondrite)/(Lasample/Lachondrite)^{1/2}\ (Prsample/Prchondrite)^{1/2},$$

$$Eu/Eu^{*}cn = (Eusample/Euchondrite)/(Smsample/Smchondrite)^{1/2}\ (Gdsample/Gdchondrite)^{1/2},$$

$$(La/Yb)cn = (Lasample/Lachondrite)/(Ybsample/Ybchondrite),$$

$$(La/Sm)cn = (Lasample/Lachondrite)/(Smsample/Smchondrite),$$

$$(Gd/Yb)cn = (Gdsample/Gdchondrite)/(Ybsample/Ybchondrite).$$

4.4. Source area weathering

Feldspars and other primary minerals from crystalline bedrocks are gradually converted into clays, secondary oxides, and hydroxides during weathering processes [29,39]. The rate of transformation in relation to the degree of weathering, as well as other factors like paleoclimate and tectonism, is vital. Weathering indices have been developed to characterize chemical weathering in sediments and soils [29–31]. The degree of weathering is linked to the mobility of cations such as Na^{+}, K^{+}, and Ca^{2+} during chemical weathering processes. The present study measured source area weathering by various weathering indices, including the Chemical Index of Alternation (CIA), Chemical Index of Weathering (CIW), and Plagioclase Index of Alteration (PIA) [29,31,39,40]. The source area weathering of the soils under study was also inferred using elemental ratios. The weathering indices values are presented in **Table 1** above. The CIA values of the studied soil samples indicate a moderate degree of weathering (CIA 50–70; **Table 1**). The PIA index is more appropriate for the study because it takes into consideration the impact of K-bearing feldspar (orthoclase and microcline), whereas potash feldspars show distinct weathering behaviors from plagioclase. The PIA value varies from 77.03 to 97.75 (**Table 1**; **Figure 2**), which indicates intense plagioclase degradation in all soil samples and shows intense weathering in the source area. This result is consistent with CIW (91.31–99.13%) values, revealing a high weathering intensity. This is different from utilizing the molar concentration of numerous oxides found in the soils. In general, PIA values tend to be higher, and they frequently tend to be greater. Significant weathering in the source area and a widespread process of bisiallitization are indicated by the Ruxton index (SiO_2 (adj)/Al_2O_3 ratio) values, which vary from 4.23 to 5288.07 (**Table 1**). The soil samples' CIA and CIX values indicate a moderate level of weathering in the source area (**Table 1**), while the CIW (91.31%–99.13%) and PIA (77.03%–97.75%) values show high intensity of weathering in the source area (**Table 1**; **Figure 2)**, which produces residual clay that is abundant in kaolinite, gibbsite, chlorite, and Al-oxihydroxides. The lack of recent tectonic activity supports intense chemical weathering and modest erosion rates, which are aided by significant seasonal rains in the study area. According to **Table 1**, the soil samples have high K_2O/Na_2O ratios (14.37 to 204.77), which suggest that the source's area has experienced intense weathering. The soil samples also displayed high ΣREE values, which indicate high weathering intensity in the study area (**Table 4**). The breakdown of feldspars during weathering, transportation, and pedogenesis is supported by the high values for CIW and PIA (> 80). The low percentage of detrital

feldspars and the presence of clay minerals are likely the causes of the high CIW and PIA values, which may suggest that the parent rocks from which the soils were formed underwent both physical and chemical weathering [2]. This finding suggests that the CIA and CIX, as well as the PIA and CIW indices, behave similarly for the various parent materials. This implies that the soils come from bedrock that is felsic and mafic in composition. The local geology of the study area has a significant impact on the soil weathering and composition. The non-steady-state weathering indicates balanced rates of erosion and chemical weathering, which over time result in soils with comparable compositions. In order to determine the weathering history of sediments, several authors have employed the Th/U ratio, which indicates the extent of uranium oxidation and loss during weathering [41,42]. Soil Th/U ratios range from 1 to 5.77, with an average of 2.85, indicating that the soil is above the Upper Continental Crust value (**Table 3**). The parent rocks of these soils have undergone the most weathering. Weathering and sedimentary processes are known to cause Ce to fractionate [43]. In the early phases of weathering, weathering products like secondary hydrous phosphates exhibit negative Ce anomalies [44], while heavily weathered lateritic profiles exhibit positive Ce anomalies, where soluble Ce^{3+} oxidizes to insoluble, thermodynamically stable Ce^{4+} and accumulates in minerals like secondary cerianite and CeO_2 [45]. The relatively high Ce anomalies in the soil samples (Ce/Ce* = 0.01 to 7.44) (**Table 4**) suggest that the chemical weathering experienced by the soil was more intensive. The Mount Bamboutos soil reflects moderate to high weathering conditions as determined from CIA, PIA, CIW, and CIX indices (**Table 1**), and the intense chemical alteration reflects hot and humid climatic conditions [46]. Based on the log (Fe_2O_3/Al_2O_3) versus log (Fe_2O_3/K_2O) binary plot (**Figure 3**), the samples are classified as litharenite and wacke. According to similar research, the Meghna and Brahmaputra sediments [47,48] were mainly composed of litharenite, with SiO_2 concentrations varying between 58 and 80 weight percent.

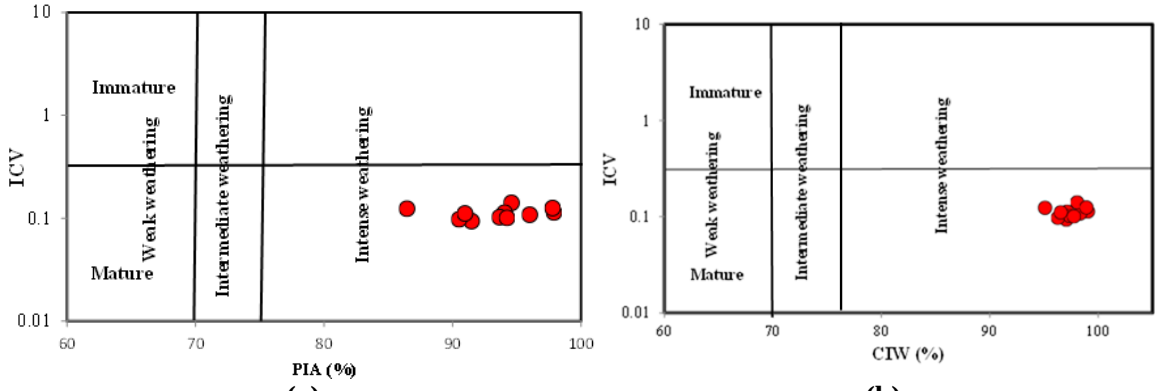

Figure 2. Bivariate plots of ICV versus PIA and ICV versus CIW.

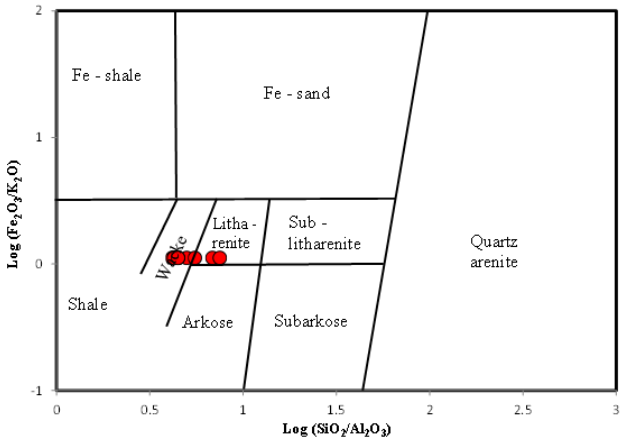

Figure 3. Geochemical classifications of the Bamboutos soils using a log (Fe_2O_3/Al_2O_3) versus log (Fe_2O_3/K_2O) diagram.

5. Conclusions

The weathering of the source area was constrained using the geochemical data for soil samples. In conjunction with the geology of the study area, the enrichment of Fe_2O_3 indicates a ferruginous nature and the origin of soils from rocks that are rich in iron. SiO_2 (adj) and Al_2O_3 have negative associations, which suggests that the relative amount of quartz mostly controls the primary element composition of the soils. The depletion in HFSE and LILE was probably due to weathering intensity. PIA, CIW, CIX, the Ruxton index, and CIA all indicate that moderate to intense weathering predominates in hot, humid climates in the source area. The soils are dominantly made up of litharenite and wacke. The relatively high Ce anomalies in the soil samples (Ce/Ce* = 0.01 to 7.44; average 2.39) suggest that the chemical weathering experienced by the soil was more intensive.

Author contributions: Conceptualization, LPY and KNGD; methodology, CTB; software, EEM; validation, KNGD, LPY and ARM; formal analysis, ARM; investigation, LPY; resources, KNGD; data curation, CTB and ARM; writing—original draft preparation, LPY; writing—review and editing, EEM; visualization, CTB; supervision, KNGD; project administration, LPY; funding acquisition, KNGD. All authors have read and agreed to the published version of the manuscript.

Acknowledgments: Special appreciations are extended to anonymous reviewers for their valuable feedback and recommendations for enhancing this paper.

Conflict of interest: The authors declare no conflict of interest.

References

1. Temga JP, Azinwi Tamfuh P, Basga Djakba S, et al. Characteristics, classification and genesis of vertisols under seasonally contrasted climate in the Lake Chad Basin, Central Africa. Journal of African Earth Sciences. 2019; 150: 176-193. doi: 10.1016/j.jafrearsci.2018.11.003
2. Azinwi PT, Temga JP, Temgoua E, et al. Characteristics, Source Area-weathering, Sedimentary Processes, Tectonic Setting and Taxonomy of Vertisols Developed on Alluvial Sediments in the Benue Trough of North Cameroon. Journal of Geosciences and Geomatics. 2022; 10(1): 1-17. doi: 10.12691/jgg-10-1-1

3. Yan Y, Yang Y. Uncertainty assessment of spatiotemporal distribution and variation in regional soil heavy metals based on spatiotemporal sequential Gaussian simulation. Environmental Pollution. 2023; 322: 121243. doi: 10.1016/j.envpol.2023.121243
4. Dengiz O, Usul M. Multi-criteria approach with linear combination technique and analytical hierarchy process in land evaluation studies. Eurasian Journal of Soil Science (EJSS). 2018; 7(1): 20-29. doi: 10.18393/ejss.328531
5. Azinwi TP, Djoufac Woumfo E, Temgoua E, et al. Moisture content, moisture-related properties and agricultural management strategies of the Benue floodplain vertisols in North Cameroon. African Journal of Agricultural Research. 2018; 13(33): 1730-1746. doi: 10.5897/ajar2018.13349
6. Yiika LP, Tita MA, Suh CE, et al. Heavy Metal Speciation by Tessier Sequential Extraction Applied to Artisanal Gold Mine Tailings in Eastern Cameroon. Chemistry Africa. 2023; 6(5): 2705-2723. doi: 10.1007/s42250-023-00652-0
7. Yiika LP, Jean-Lavenir NM, Monespérance MGM, et al. Contamination and risk assessment of heavy metals in stream sediments of Bambui area, western Cameroon. International Journal of Research and Innovation in Applied Science. 2022; 7(11): 64-75.
8. Afahnwie NA, Embui VF, Yiika LP, et al. Preliminary stream sediment geochemical exploration for base metals and other elements in terms of source apportionment and contamination status of Manjo and environs, Cameroon. Discover Chemistry. 2025; 2(1). doi: 10.1007/s44371-025-00183-2
9. Ndema Mbongué JL, Sigué C, Igor Fulbert MN, et al. Potentially toxic metals contamination in stream sediments of Mbal area (Pan-African fold belt, Cameroon). Discover Geoscience. 2024; 2(1). doi: 10.1007/s44288-024-00017-1
10. Ndema Mbongué JL, Tume NK, Yiika LP, et al. Contamination, sources and risk assessments of metals in stream sediments of Pouma area, Pan-African Fold Belt, Southern Cameroon. Water, Air, & Soil Pollution. 2023; 234(3). doi: 10.1007/s11270-023-06180-4
11. Tiabou AF, Takem-Agbor AA, Yiika LP, et al. Distribution, source apportionment and ecological risk assessment of heavy metals in Limbe River sediments, Atlantic Coast, Cameroon Volcanic Line. Discover Water. 2024; 4(1). doi: 10.1007/s43832-024-00120-x
12. Tiabou AF, Atabe GAA, Sigue C, et al. Appraisal of pollution, ecological and health risks assessment of trace metals in soils of Logbadjeck quarrying area, Nyong Series, Cameroon. Journal of Trace Elements and Minerals. 2024; 10: 100204. doi: 10.1016/j.jtemin.2024.100204
13. Tiabou AF, Mboudou GMM, Ghanyuymo MM, et al. Evaluation of surface and groundwater quality in Logbadjeck quarrying area: implications for trace metals pollution and health risk assessment. International Journal of Energy and Water Resources. 2025; 9(2): 893-915. doi: 10.1007/s42108-024-00321-z
14. Tiabou AF, Tanyi TAM, Yiika LP, et al. Spatial distribution, ecological and ecotoxicity evaluation of heavy metals in agricultural soils along Lala-Manjo Highway, Cameroon Volcanic Line. Discover Soil. 2024; 1(1). doi: 10.1007/s44378-024-00010-7
15. Tiabou AF, Esuka CN, Mbowou Ngantche IF, et al. Spatial Distribution, Contamination Characteristics and Eco-Risk Assessment of Toxic Metals in Stream Sediments of Njombe-Penja Banana Plain, Cameroon Volcanic Line. Chemistry Africa. 2025; 8(2): 619-639. doi: 10.1007/s42250-024-01159-y
16. Suh GC, Afahnwie NA, Tiabou AF, et al. Source apportionment, ecological and toxicological risk assessment of trace metals in agricultural soils of Wabane, South West Region, Cameroon. Journal of Trace Elements and Minerals. 2025; 12: 100218. doi: 10.1016/j.jtemin.2025.100218
17. Hasan O, Miko S, Mesić S, et al. Chemical Weathering Rates of Soils Developed on Eocene Marls and Sandstones in a Mediterranean Catchment (Istria, Croatia). Land. 2023; 12(4): 913. doi: 10.3390/land12040913
18. Gonçalves DAM, Pereira WV da S, Johannesson KH, et al. Geochemical Background for Potentially Toxic Elements in Forested Soils of the State of Pará, Brazilian Amazon. Minerals. 2022; 12(6): 674. doi: 10.3390/min12060674
19. Youmen D. Volcanological, petrological and temporal evolution of the Bambouto caldera (Cameroun). Allemagne: Christian-Albrechts-Universität zu Kiel; 1994; 274p + 2 Cartes.
20. Nguetnkam JP, Kamga R, Villiéras Ekodeck GE, Yvon J. Weathering response of granite in tropical zones. Example of two sequences studied in Cameroon (Central Africa). Etude et Gestion des Sols. 2007; 14(1): 13-41.
21. Déruelle B, Ngounouno I, Demaiffe D. The 'Cameroon Hot Line' (CHL): A unique example of active alkaline intraplate structure in both oceanic and continental lithospheres. Comptes Rendus Géoscience. 2007; 339(9): 589-600. doi: 10.1016/j.crte.2007.07.007

22. Nono A, Njonfang E, Kagou Dongmo A, et al. Pyroclastic deposits of the Bambouto volcano (Cameroon Line, Central Africa): evidence of an initial strombolian phase. Journal of African Earth Sciences. 2004; 39(3-5): 409-414. doi: 10.1016/j.jafrearsci.2004.07.026
23. Gountié Dedzo M, Diddi Hamadjoda D, Fozing EM, et al. Petrology and geochemistry of ignimbrites and associated enclaves from Mount Bambouto, West-Cameroon, Cameroon Volcanic Line. Geochemistry. 2020; 80(4): 125663. doi: 10.1016/j.chemer.2020.125663
24. Nni J, Nyobe JB. Geology and petrology of the precalderic lavas of the Bambouto Mountains: Cameroon Line (French). Geochemica Brasiliensis. 1995; 9(1): 47-59.
25. Gountié Dedzo M, Nédélec A, Nono A, et al. Magnetic fabrics of the Miocene ignimbrites from West-Cameroon: Implications for pyroclastic flow source and sedimentation. Journal of Volcanology and Geothermal Research. 2011; 203(3-4): 113-132. doi: 10.1016/j.jvolgeores.2011.04.012
26. Merle R, Marzoli A, Aka FT, et al. Mt Bambouto Volcano, Cameroon Line: Mantle Source and Differentiation of Within-plate Alkaline Rocks. Journal of Petrology. 2017; 58(5): 933-962. doi: 10.1093/petrology/egx041
27. Rudnick RL, Gao S. The composition of the continental crust. Treatise on Geochemistry. 2003; 3: 1-64. doi: 10.1016/B0-08-043751-6/03016-4
28. McLennan SM. Rare earth elements in sedimentary rocks: influence of provenance and sedimentary processes. In: Geochemistry and Mineralogy of Rare Earth Elements. De Gruyter; 1989.
29. Nesbitt HW, Young GM. Prediction of some weathering trends of plutonic and volcanic rocks based upon thermodynamic and kinetic consideration. Geochimica et Cosmochimica Acta. 1984; 48(7): 1523-1534. doi: 10.1016/0016-7037(84)90408-3
30. Cox R, Low DR, Cullers RL. The influence of sediment recycling and basement composition on evolution of mudrock chemistry in the southwestern United States. Geochimica et Cosmochimica Acta. 1995; 59(14): 2919-2940. doi: 10.1016/0016-7037(95)00185-9
31. Harnois, L. The CIW index: A new chemical index of weathering. Sedimentary Geology. 1988; 55(3-4): 319-322. doi: 10.1016/0037-0738(88)90137-6
32. Ruxton BP. Measures of the Degree of Chemical Weathering of Rocks. The Journal of Geology. 1968; 76(5): 518-527. doi: 10.1086/627357
33. Yiika LP, Jean-Lavenir NM, Suh GC, et al. Distribution, Sources, and Eco-toxicological Assessment of Potentially Toxic Metals in River Sediments of Nkwen Area (Cameroon Volcanic Line). Water, Air, & Soil Pollution. 2023; 235(1). doi: 10.1007/s11270-023-06830-7
34. Kouankap Nono GD, Yiika LP, Etutu EMM, et al. Geochemistry of sediments from the Mugheb River, Bamenda, Cameroon Volcanic Line: implications for provenance, paleoweathering and tectonic setting. Arabian Journal of Geosciences. 2024; 17(12). doi: 10.1007/s12517-024-12148-3
35. Ramos-Vázquez MA, Armstrong-Altrin JS, Madhavaraju J, et al. Mineralogy and geochemistry of marine sediments in the Northeastern Gulf of Mexico. In: Geochemical Treasures and Petrogenetic Processes. Springer; 2022.
36. Xie Y, Chi Y. Geochemical investigation of dry- and wet-deposited dust during the same dust-storm event in Harbin, China: Constraint on provenance and implications for formation of aeolian loess. Journal of Asian Earth Sciences. 2016; 120: 43-61. doi: 10.1016/j.jseaes.2016.01.025
37. Armstrong-Altrin JS, Nagarajan R, Balaram V, et al. Petrography and geochemistry of sands from the Chachalacas and Veracruz beach areas, western Gulf of Mexico, Mexico: Constraints on provenance and tectonic setting. Journal of South American Earth Sciences. 2015; 64: 199-216. doi: 10.1016/j.jsames.2015.10.012
38. Rahman MA, Das SC, Pownceby MI, et al. Geochemistry of Recent Brahmaputra River Sediments: Provenance, Tectonics, Source Area Weathering and Depositional Environment. Minerals. 2020; 10(9): 813. doi: 10.3390/min10090813
39. Fedo CM, Nesbitt HW, Young GM. Unravelling the Aects of potassium metasomatism in sedimentary rocks and paleosols, with implications for paleoweathering conditions and provenance. Geology. 1995; 23(10): 921-924. doi: 10.1130/0091-7613(1995)023<0921:UTEOPM>2.3.CO;2
40. Jie HE, Garzanti D, PedroY, et al. Provenance versus weathering control on sediment composition in tropical monsoonal climate (South China) - 1. Geochemistry and clay mineralogy. Chemical Geology. 2020; 558: 119860. doi: 10.1016/j.chemgeo.2020.119860
41. Singh P. Major, trace and REE geochemistry of the Ganga River sediments: Influence of provenance and sedimentary processes. Chemical Geology. 2009; 266(3-4): 242-255. doi: 10.1016/j.chemgeo.2009.06.013

42. Gu XX, Liu JM, Zheng MH, et al. Provenance and Tectonic Setting of the Proterozoic Turbidites in Hunan, South China: Geochemical Evidence. Journal of Sedimentary Research. 2002; 72(3): 393-407. doi: 10.1306/081601720393
43. Borges JB, Huh Y, Moon S, et al. Provenance and weathering control on river bed sediments of the eastern Tibetan Plateau and the Russian Far East. Chemical Geology. 2008; 254(1-2): 52-72. doi: 10.1016/j.chemgeo.2008.06.002
44. Braun JJ, Viers J, Dupré B, et al. Solid/liquid REE fractionation in the lateritic system of Goyoum, East Cameroon: The implication for the present dynamics of the soil covers of the humid tropical regions. Geochimica et Cosmochimica Acta. 1998; 62(2): 273-299. doi: 10.1016/S0016-7037(97)00344-X
45. Pan Y, Stauffer MR. Cerium anomaly and Th/U fractionation in the 1.85 Ga Flin Flon Paleosol: Clues from REE- and U-rich accessory minerals and implications for paleoatmospheric reconstruction. American Mineralogist. 2000; 85(7-8): 898-911. doi: 10.2138/am-2000-0703
46. Etemad-Saeed N, Hosseini-Barzi M, Armstrong-Altrin JS. Petrography and geochemistry of clastic sedimentary rocks as evidences for provenance of the Lower Cambrian Lalun Formation, Posht-e-badam block, Central Iran. Journal of African Earth Sciences. 2011; 61(2): 142-159. doi: 10.1016/j.jafrearsci.2011.06.003
47. Bhuiyan MAH, Rahman MJJ, Dampare SB, et al. Provenance, tectonics and source weathering of modern fluvial sediments of the Brahmaputra–Jamuna River, Bangladesh: Inference from geochemistry. Journal of Geochemical Exploration. 2011; 111(3): 113-137. doi: 10.1016/j.gexplo.2011.06.008
48. Hossain HMZ. Major, trace, and REE geochemistry of the Meghna River sediments, Bangladesh: Constraints on weathering and provenance. Somerville I, ed. Geological Journal. 2019; 55(5): 3321-3343. doi: 10.1002/gj.3595